Journal of Fluids and Structures (2001) **15,** 955–980
doi:10.1006/jfls.2001.0382, available online at http://www.idealibrary.com on IDEAL®

CROSS-FLOW PAST AN OSCILLATING CIRCULAR CYLINDER: SYNCHRONIZATION PHENOMENA IN THE NEAR WAKE

S. Krishnamoorthy, S. J. Price and M. P. Païdoussis

Department of Mechanical Engineering, McGill University, 817 Sherbrooke Street West Montreal, Québec, Canada H3A 2K6

(Received 10 August 2000, and in final form 3 May 2001)

Cross-flow past a circular cylinder in a water tunnel undergoing forced harmonic oscillations in the transverse plane was investigated experimentally at Reynolds numbers ranging from 1250 to 1500, by means of dye visualization of the formation region and measurement of wake spectra. Cylinder oscillation frequencies f_e ranging from $\frac{1}{3}$-subharmonic excitation to 3-superharmonic excitation were considered, with the amplitude of oscillation fixed at 0·22 diameters. As f_e is incremented within the fundamental lock-in regime, the structure of the formation region undergoes two distinct transitions. The first transition, which is accompanied by an abrupt reduction in vortex formation length, corresponds to a switch from the '2P' wake vortex pattern to the '2S' wake vortex pattern of Williamson & Roshko. After a subsequent transition, the phase of vortex shedding relative to cylinder displacement switches by about π. Between the two transitions, the vortex formation length is a minimum. A similar minimum seems to be next attained only when f_e is increased to achieve 3-superharmonic synchronization. Finally, while for both the $\frac{1}{3}$-subharmonic excitation and the $\frac{1}{2}$-subharmonic excitation the topology of the formation region is periodic with every cycle of cylinder oscillation, a synchronized wake pattern forms only in the former case.

1. INTRODUCTION

This experimental investigation of the near-wake structure and its evolution from a circular cylinder in cross-flow subjected to forced simple-harmonic oscillation in the transverse plane is relevant to many practical applications in which flow-induced vibration of cylindrical structures subjected to cross-flow is manifest. Typical applications such as flow past heat exchanger tubes, power transmission lines subjected to cross-wind, marine risers, etc. are discussed in the reviews of Blevins (1977), Païdoussis (1980, 1981, 1983, 1993) and Chen (1987a, b). Flow-induced vibration of an elastically mounted cylinder in cross-flow is determined by the dynamic fluid forces acting on it. Details are available in classic articles such as those of Mair & Maull (1971a), Sarpkaya (1979), Bearman (1984) and Parkinson (1989). Vortex shedding and the consequent fluctuating lift force induces transverse oscillations of the cylinder (in-line vortex-induced vibrations are also possible). In turn, the fluctuating lift force due to vortex shedding from a stationary cylinder in cross-flow is substantially modified when the cylinder oscillates; i.e., the vortex shedding process is modified by cylinder oscillation. Investigation of the structure of the near-wake and of the vorticity dynamics therein, as well as the relationship to the cylinder motion by means of forced oscillation experiments, is important in improving our understanding of the modification of fluctuating lift force due to cylinder oscillation.

0889–9746/01/070955 + 26 $35.00/0

The problem of cross-flow past an oscillating circular cylinder has been studied from a variety of different perspectives, at various Reynolds numbers ranging from hundreds to millions. Classically, the focus has been on the phenomenon of 'lock-in', where the frequency of vortex shedding is synchronized with the frequency of oscillation of the cylinder. The lock-in phenomenon has been studied both for the case of an elastically mounted cylinder in cross-flow [e.g., by Feng (1968), and more recently by Brika & Laneville (1993) and Khalak & Williamson (1996, 1997)], and for the case of forced simple-harmonic oscillation of a cylinder in cross-flow in the transverse plane of the flow [e.g., Den Hartog (1934), Bishop & Hassan (1964), Koopman (1967), Stansby (1976), Bearman & Currie (1979), Williamson & Roshko (1988), Ongoren & Rockwell (1988), Lu & Dalton (1996) and Blackburn & Henderson (1999)].

In their introductory discussion, Blackburn & Henderson (1999) describe the phenomenon of lock-in as the result of an entrainment process, in which vortex shedding is entrained by the cylinder motion, so that the vortex shedding frequency matches the cylinder oscillation frequency. They also discuss how entrainment/lock-in behaviour for the vibration of elastically mounted cylinders differs from that for forced oscillation. In the former, fluid-structure coupling occurs in both directions, while in the latter the cylinder motion is constrained. While the mechanical energy transferred from the flow to the oscillating cylinder per cycle may be positive or negative for forced oscillation, its long-term average must be positive for an elastically mounted cylinder.

Some of the most relevant previous forced oscillation studies are discussed in what follows to provide the necessary background for the current study. The relevant parameters governing such studies are: (i) Reynolds number, $\mathrm{Re} = UD/\nu$; (ii) amplitude ratio, A/D; (iii) frequency ratio, f_e/f_{0s}; (iv) reduced frequency, $f_e D/U$, or reduced velocity, $U/f_e D$; where U is the freestream velocity, D the cylinder diameter, ν the kinematic viscosity of the fluid, and A and f_e are the amplitude and frequency of oscillation of the cylinder, respectively. The vortex shedding (Strouhal) frequency for the stationary cylinder is denoted by f_{0s}, while for the oscillating cylinder it is denoted by f_0. In addition to these parameters, cylinder end-effects, tunnel blockage, surface finish and freestream turbulence levels are also important.

The wake structure from a cylinder forced to undergo transverse oscillations in cross-flow at low Reynolds numbers (less than 350), within the locked-in regime, has been studied extensively by Koopman (1967), Griffin (1971), Griffin & Votaw (1972) and Griffin & Ramberg (1974). Koopman (1967) determined a threshold (minimum) oscillation amplitude of $A/D = 0{\cdot}05$ required for lock-in. Above this threshold amplitude, coherence of the separation points along the cylinder span is induced, and slant-wise vortex shedding is replaced by parallel vortex shedding. Griffin & Ramberg (1974) obtained the vortex formation length, vortex strength and vortex spacing through the lock-in range. Phenomena such as suppression of turbulence-initiation downstream of vortex formation, and extension of the laminar stable vortex street regime to a higher Reynolds number due to cylinder oscillation in the locked-in regime, are discussed in Griffin (1971) and Griffin & Votaw (1972).

Vortex shedding behind an oscillating cylinder at the higher Reynolds numbers pertaining to our study (> 350) is a turbulent process. At $\mathrm{Re} = 6000$ and $A/D = 0{\cdot}25$, Bishop & Hassan (1964) showed that the most significant feature of fluid–structure interaction during forced oscillation of a circular cylinder at frequencies within the locked-in regime is the large increase in vortex-induced forces on the cylinder with increasing frequency, followed by a discontinuous drop in force in the middle of the locked-in range. The value of the critical forcing frequency at which the discontinuity occurred depended on whether the frequency was incrementally increased or decreased, displaying hysteretic behaviour. The

jump in magnitude was also accompanied by a jump in the phase of the fluctuating force with respect to cylinder motion. Bearman & Currie (1979) also observed similar phenomena in their measurements of fluctuating side pressure (at the shoulder of the cylinder).

Zdravkovich (1982) mentions three causes for the magnification of fluctuating forces on the oscillating cylinder within the locked-in (synchronized) regime, based on prevalent notions: (a) shortening of vortex formation length, as discussed by Gerrard (1966) for turbulent wakes; (b) increase in spanwise correlation of the vortex shedding process, measured by Toebes (1969); (c) increased period of vortex shedding giving rise to stronger vortices (Sarpkaya 1979). Based on analysis of earlier published flow visualization results, Zdravkovich concludes that, within the synchronization range, the timing of vortex shedding with respect to cylinder motion undergoes a sudden jump (corresponding to a phase difference of about π).

Stansby (1976) measured the vortex shedding frequency from a circular cylinder forced to oscillate transversely in a uniform flow with Reynolds numbers spanning the range 3600–9200. Spectral measurements using a hot wire probe, combined with the cylinder displacement signal, were used to characterize vortex shedding and its phase relationship to cylinder displacement. Besides the fundamental locked-in regime ($f_0 = f_e$), results for a 'secondary' locked-in regime ($f_0 = \frac{1}{2} f_e$) corresponding to '2-superharmonic' forcing, and a 'tertiary' locked-in regime ($f_0 = \frac{1}{3} f_e$) corresponding to '3-superharmonic' forcing were also obtained. While tertiary lock-in occurred over a wide range of forcing frequencies, secondary lock-in did not. At the boundaries of the primary locked-in regime, locked-in shedding was intermittent with unforced shedding. Within the locked-in range, the critical frequency corresponding to the phase jump (of approximately π), was obtained for various A/D.

Williamson & Roshko (1988) visualized the wake structure behind a towed circular cylinder subjected to transverse forcing using aluminium particles on the free surface, and developed a regime map based on visualized wake patterns, with Reynolds numbers ranging from 300 to 1000. The parameter space $0{\cdot}2 < A/D < 1{\cdot}8$ and $1{\cdot}0 < U/f_eD < 10{\cdot}0$, which spanned the fundamental lock-in region, was studied in detail with a view to explain the jump in fluctuating fluid forces and their phase with respect to cylinder motion. As U/f_eD was increased, they observed a sudden change in synchronized vortex shedding from a '2S' mode (where two single vortices were shed per cycle of cylinder oscillation giving rise to a Karman type vortex street) to a '2P' mode (where four vortices were shed per cycle of cylinder oscillation giving rise to a vortex street composed of two vortex pairs). This abrupt mode-change was proposed as the cause of the jump in the force. The 2S and 2P modes were demarcated by a critical curve close to $U/f_eD = 5$ (or $f_e/f_{0s} = 1$). As U/f_eD was increased past the 2S and 2P regimes, no synchronized vortex pattern was observed until the oscillation frequency corresponded to a $\frac{1}{3}$-subharmonic forcing ($f_e/f_{0s} = 1/3$), where a 2P + 2S type synchronized vortex pattern comprising six vortices (two vortex pairs and two single vortices) was observed. The reason why a synchronized vortex pattern of four vortices, corresponding to $\frac{1}{2}$-subharmonic forcing, is not possible is explained using symmetry arguments. The mechanism of vortex formation governing the mode change from 2S to 2P is addressed. Acceleration of the cylinder every half cycle (from one end of the stroke to the other) causes vortex roll-up from each shear layer. Thus four vortices are formed from the shear layers for every cycle of oscillation. The 2S pattern is formed when the timing of vortex roll-up is such that two like-sign vortices coalesce to give rise to two vortices per cycle of cylinder oscillation. When the timing of vortex formation is such that vortices of opposite sign pair up to give rise to two vortex pairs per cycle, the 2P pattern results. At the critical oscillation frequency, the timing is such that only two vortices are formed per cycle, and the shed vortices are the most coherent (2S type). This wake condition is referred to as 'resonant synchronization'.

Ongoren & Rockwell (1988) conducted forced oscillation experiments in a water channel, mostly at Re = 855, with cylinders of various cross-sections. Wake spectra and the phase of vortex shedding with respect to cylinder displacement were measured over a wide range of frequency ratios, and the flow was visualized using the hydrogen bubble technique. For a circular cylinder, they found synchronization (phase-locking) of the *near-wake structure* to the cylinder motion, both for $\frac{1}{2}$-subharmonic forcing ($f_e/f_{0s} = 1/2$) when vortex shedding from the shear layers repeats with every half-cycle of cylinder displacement, and for harmonic forcing ($f_e/f_{0s} = 1$) when vortex shedding repeats with every full cycle. The perturbed near-wake was observed to recover rapidly to an antisymmetric Karman vortex street over a wide range of oscillation frequencies, varying from subharmonic to 4-superharmonic ($f_e/f_{0s} = 4$) forcing. The frequency f_0 of the recovered vortex street showed substantial departure from f_{0s}, locking onto resonant modes corresponding to $f_0/f_e = 1/n$, $n = 1, 1{\cdot}5$, 2, 3 and 4. The phase jump of vortex formation with respect to cylinder displacement of approximately π within the fundamental synchronization (lock-in) regime is well illustrated in their flow visualizations.

Gu *et al.* (1994) studied the phase switch phenomenon by means of particle imaging velocimetry. Results for the critical oscillation frequency at which the phase switch occurred (Re = 5000 with $A/D = 0{\cdot}2$) compared favourably with those of Bishop & Hassan for phase switching of the fluctuating lift force. The phase switch phenomenon was also observed in later numerical studies, such as those of Lu & Dalton (1996) and Blackburn & Henderson (1999). Blackburn & Henderson conducted a 2-D simulation with Re = 500 and $A/D = 0{\cdot}25$. They observed several complex wake states within the locked-in regime. When the wake is in a periodic state prior to the phase switch ($f_e/f_{0s} = 0{\cdot}875$), energy transfer from the fluid to the cylinder, averaged over a cycle, is shown to be positive. For periodic states of the wake after the phase switch, the energy transfer is negative. In the region between these two periodic wake states ($0{\cdot}905 < f_e/f_{0s} < 0{\cdot}95$), termed the 'weakly chaotic relaxation oscillator regime', the wake slowly switched states in an almost periodic manner with the average energy transfer being either positive or negative.

In the present study, excitation frequencies spanned a wide range from $\frac{1}{3}$-subharmonic to 3-superharmonic. A combination of flow visualization by means of dye injection into the shear layers and wake spectra measurements using a hot film probe was employed, with the amplitude ratio fixed at $A/D = 0{\cdot}22$. The Reynolds number range pertaining to our study (1250–1500) is most suited for the purpose of resolving the fundamental lock-in regime. Also, at higher Reynolds numbers, over 2500, the shear layers are unstable and vortex formation in the wake is turbulent. Dye visualization of vortex formation is not available in the literature, except at lower Reynolds numbers, less than 350, where the near-wake dynamics is dominated by viscous forces. The current study is comparable, in terms of Reynolds number, to those of Williamson & Roshko, Ongoren & Rockwell, and to a lesser extent that of Stansby.

The present investigation of the near-wake of an oscillating cylinder is our initial step towards understanding the complex flow phenomena generated when a second circular cylinder is introduced in the vicinity of the forced cylinder. A classical analysis of the behaviour of bodies immersed in bluff body wakes is available in an insightful article by Mair & Maull (1971b).

2. EXPERIMENTAL SET-UP

Experiments were conducted in a closed circuit, recirculating Kempf & Remmers water tunnel, which has a 110 cm long test-section, 260 mm × 260 mm in cross-section [details are available in Price & Serdula (1995)]. Flow in the test-section has a streamwise turbulence

intensity of 0·5% and a velocity profile uniformity of better than 95%. A circular cylinder of diameter $D = 15{\cdot}9$ mm (aspect ratio of 16·4, solid blockage ratio of 6·2%) was used. The freestream velocity U was measured using a miniature current "turbine" flowmeter, designed for very low flow velocities in water (40–150 mm/s).

The cylinder was mounted vertically from above the test-section. The arrangement of the cylinder in the test-section and the apparatus for achieving forced harmonic oscillation in the transverse plane are illustrated in Figure 1. The cylinder (made of solid extruded Plexiglas rod) was rigidly clamped to a linear traverse table constrained to move in the plane perpendicular to the freestream. The traverse table was forced to oscillate back and forth with a sinusoidal profile, by means of a "Scotch–Yoke" linkage. The Scotch–Yoke mechanism converted the rotary motion of the drive shaft into sinusoidal motion of the traverse table. The entire mechanism was mounted in a pressure-sealed housing above the test-section, so that the oscillating cylinder protruded into the test-section, clamped at the top end and free at the bottom end. The gap between the free end of the cylinder and the test-section bottom was around 0·5–1·0 mm. The length of the cylinder, from clamped end to free end, was 268 mm, of which 260 mm projected into the test-section.

A DC servomotor powered the drive shaft via a 6:1 reduction gearbelt–pulley system. Closed-loop feedback control was achieved by means of an in-line optical encoder and a digital driver set for speed control. With this system, the oscillation frequency of the cylinder, f_e, could be set in the range 0·2–4·86 Hz (motor speed range of 72 r.p.m.–1750 r.p.m.). The instantaneous r.p.m. of the motor varied by about ± 1 r.p.m. at any set r.p.m. in this range.

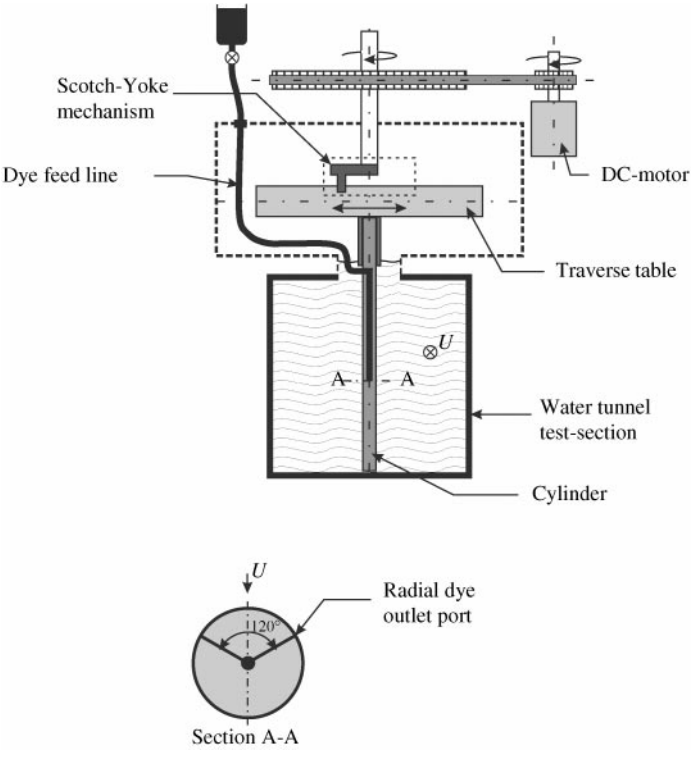

Figure 1. Sketch of the experimental set-up illustrating the mechanism by which forced harmonic oscillation of the cylinder is achieved. Details pertaining to dye injection into the cylinder boundary layer are also shown.

The displacement profile of the oscillating cylinder was measured by tracking the motion of its free end using an electro-optical displacement follower. This was done in order to assess the accuracy of the drive system in providing sinusoidal motion to the cylinder. The resulting time traces indicated that there was some dwell at the ends of the stroke for low oscillation frequencies, ranging from 0·1 to 0·5 Hz. This dwell became negligible at higher oscillation frequencies, and the effect of knocking in the traverse table became predominant. However, the power ratio of the knocking frequency to that of the oscillation frequency was only of order 10^{-3}–10^{-4}. These inaccuracies were deemed sufficiently small, while the motion of the cylinder was adequately sinusoidal for our purposes, over the desired range of oscillation frequencies. From the time traces, the stroke of the oscillating cylinder ($2A$) was determined to be 7·0 mm, and remained fixed in these experiments. Therefore, we have an amplitude ratio $A/D = 0{\cdot}22$.

Flow visualization was carried out by means of a fluorescent dye (Rhodamine) injected into the boundary layer of the cylinder in the plane bisecting the test-section and normal to the cylinder axis (see Figure 1). This mid-plane of the test-section (where the dye is released) was illuminated by a light sheet from a Xenon arc lamp about 12–15 mm thick. Dye was gravity-fed into the cylinder boundary layer through a pair of 0·34 mm diameter radial dye ports 120° apart. The dye ports were oriented such that they were facing upstream and symmetrically located with respect to the freestream. The dye flow rate was controlled by means of a needle valve in the gravity feed line. The wake structure revealed by the dye was recorded on analog video tape (NTSC standard, 30 frames per second) using a professional S-VHS video camera.

A TSI Flowpoint (model 1500) anemometer system, consisting of a two-channel velocity transducer, a type-1269W single component hot-film probe (with a recommended velocity range of 0·03–30 m/s) and associated hardware and software, was used to determine the frequencies in the near wake of the oscillating cylinder. The probe was calibrated in the water tunnel for a maximum velocity of 0·35 m/s. The output from the velocity transducer was fed directly into a dynamic signal analyser (Hewlett-Packard, model 3562A) in order to obtain the velocity power spectra. The measured spectra had a frequency resolution of 12·5 mHz, and a Hanning window was used. Spectra from four samples (total sampling time of 5·33 min) were r.m.s.-averaged to obtain the final result at each f_e.

3. RESULTS FOR WAKE SPECTRA

The frequencies in the near wake, f_{wake}, were obtained as a function of oscillation frequency, ranging from $\frac{1}{3}$-subharmonic excitation to 3-superharmonic excitation, using the Flowpoint anemometer system. The hot film probe was mounted in the near-wake region at $X/D = 4{\cdot}6$, $Y/D = 0{\cdot}5$, where X is the streamwise location relative to the cylinder axis and Y is the distance along the direction of cylinder oscillation relative to the cylinder axis at its mean position. The location of the probe was chosen to be sufficiently far downstream of the vortex-formation region behind the stationary cylinder, such that all the frequencies in the near wake (including that of the vortex street, f_0) could be obtained.

The measured wake frequencies, expressed in nondimensional form as $f_{\text{wake}}D/U$, are plotted in Figure 2 as a function of dimensionless excitation frequency f_eD/U. The horizontal line passing through $f_{\text{wake}}D/U = 0{\cdot}2$ indicates the nominal Strouhal number (for a stationary cylinder). Usually more than one wake frequency was obtained at each f_e. The frequency of the dominant peak in the velocity spectrum (shown as solid symbols in Figure 2) is identified as the vortex shedding frequency, f_0, except in the range $0{\cdot}1 < f_eD/U < 0{\cdot}14$ and $0{\cdot}2 < f_eD/U < 0{\cdot}23$. For excitation frequencies in these ranges, two (or more) wake frequencies can be associated with f_0, the frequency of the vortex street (this

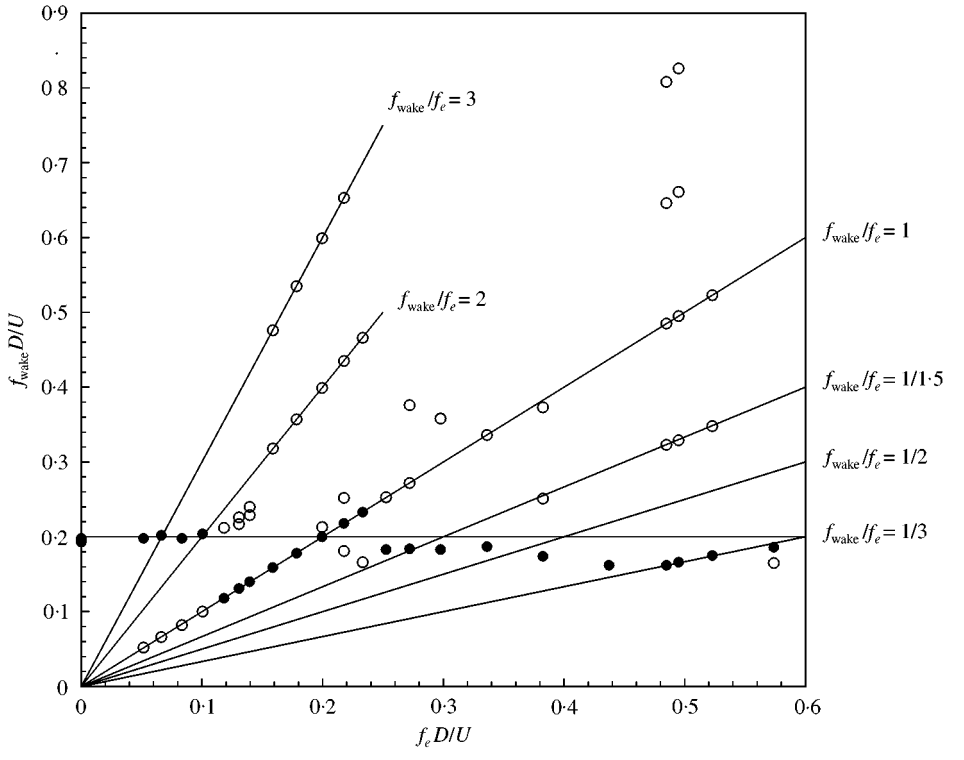

Figure 2. Dimensionless wake frequencies ($f_{wake}D/U$) as a function of dimensionless oscillation frequency (f_eD/U); ●, vortex shedding frequency; ○, remaining wake frequencies.

is discussed in greater detail in Section 4). Lines passing through the origin, of slopes 3, 2, 1, $\frac{1}{1{\cdot}5}$, $\frac{1}{2}$ and $\frac{1}{3}$, are drawn for convenience to identify the relevant sub-, non- and superharmonic wake frequencies.

The dimensionless vortex shedding frequency (f_0D/U) does not change appreciably from 0.2 in the range $0 < f_eD/U < 0{\cdot}1$, for oscillation frequencies less than that of $\frac{1}{2}$-subharmonic excitation. As f_eD/U is increased above that of $\frac{1}{2}$-subharmonic excitation, from 0·1 to 0·14, two wake frequencies occur: a dominant lower frequency $f_{wake} = f_e$, and a higher frequency $f_{wake} < 2f_e$. As discussed in Section 4.4, both of these frequencies correspond to vortex shedding. As f_eD/U is increased from 0·2 to 0·23, once again multiple wake frequencies can correspond to that of the vortex street, as the wake undergoes transition from the fundamental synchronization regime to the 1·5-nonharmonic synchronization regime. The fact that more than one wake frequency can correspond to that of vortex shedding for excitation near the boundaries of the lock-in range ($0{\cdot}1 < f_eD/U < 0{\cdot}14$ and $0{\cdot}2 < f_eD/U < 0{\cdot}23$) is consistent with the intermittent switching of the frequency of vortex shedding over several oscillation cycles, as discussed by Stansby (1976). Nevertheless, the results of this section do not provide conclusive proof of intermittent vortex shedding. Intermittent vortex shedding is, however, suggested by the flow visualization experiments discussed in Section 4. Total lock-in (fundamental synchronization) occurs for $0{\cdot}16 \leq f_eD/U \leq 0{\cdot}2$. For excitation frequencies in this range, the frequency of the dominant peak in the velocity spectrum is equal to the excitation frequency, and the other wake frequencies are superharmonics of the excitation frequency.

When f_e is increased beyond the fundamental lock-in range, f_0 is consistently less than that for the stationary cylinder. The behaviour of the vortex shedding frequency, f_0, in continuously trying to adjust itself to subsequent resonance curves as f_e is progressively increased, is discussed by Ongoren & Rockwell (1988). For excitation at frequencies above the lock-in range, we see that 3-superharmonic synchronization is clearly evident for $0{\cdot}48 < f_e D/U < 0{\cdot}52$, 1·5-nonharmonic synchronization is evident at $f_e D/U = 0{\cdot}27$, and 2-superharmonic synchronization is not evident in the spectral measurements. Superharmonics of f_0 seem to occur only within the fundamental, 1·5-nonharmonic, and 3-superharmonic synchronized regimes.

While these measurements show the variation of f_0 with f_e, and the excitation frequencies at which synchronized vortex shedding occurs, the manner in which synchronized shedding occurs is more clearly shown in the visualization experiments to be discussed in the next section.

4. RESULTS FROM FLOW VISUALIZATION

The video camera was zoomed-in to view the vortex formation region just downstream of the cylinder. The analog video recordings were then interpreted and processed both by means of conversion into digital video clips, and also by separating successive video frames into digital images. While the conversion into digital video clips was easy to do, the quality was poor. On the other hand, the digital images of successive video frames, which were of good quality, were painstakingly obtained.

A preliminary understanding of the visualization results was obtained from the digital video clips and the video tape. Separation of successive video frames into digital images enabled compilation of publishable time-sequences showing vortex evolution, vortex interactions and vortex shedding. These digital images also enabled measurement of the vortex formation length for the various cases of cylinder oscillation. In addition to the original visualization results, in order to interpret the results more clearly, dye streaks traced from relevant digital images are also presented. These tracings are scale-accurate representations of the vortex formation region, showing the shear layers and vortices in the near wake.

The vortex shedding frequency for the stationary cylinder, f_{0s}, at a freestream velocity of $U = 95$ mm/s, was determined to be 1·27 Hz (time period $T_{0s} = 0{\cdot}79$ s). The visualized vortex formation region for this case, at a time when the vortex from the lower shear layer is fully formed, is shown in Figure 3. The shear layers and the vortex roll-up, encompassing the formation region, are clearly visualized. Wake vortices are formed from the shear layers in a laminar fashion, and small-scale Kelvin–Helmholtz instability vortices are not formed on the shear layers. Figure 3 is presented primarily for comparison with visualization results for the formation region behind the oscillating cylinder.

When the cylinder was set into motion at the minimum oscillation frequency of 0·4 Hz, the shear layers developed abrupt instabilities in the form of *double roll-ups* every half-cycle of cylinder oscillation, as the cylinder moved from one end of the stroke to the other. Such vortex roll-ups, induced by cylinder acceleration every half-cycle, were observed all the way from the minimum frequency of 0·4 Hz up to 1·0 Hz. The formation of double roll-ups, starting out as abrupt kinks in the shear layers, is illustrated in both the tracings and visualization shown in Figure 4. Williamson & Roshko (1988) also observed vortex roll-ups induced every half cycle by cylinder acceleration in their experiments, with four vortices forming per cycle of cylinder oscillation within the fundamental lock-in regime. It is not clear why *double roll-ups*, as opposed to the single roll-up of Williamson & Roshko, were observed in the present experiments. However, they nominally interacted in a manner similar to that of a single roll-up in the process of generating the vortex street.

Figure 3. Image showing the visualized vortex formation region behind the stationary cylinder, when the 'lower' vortex is fully formed.

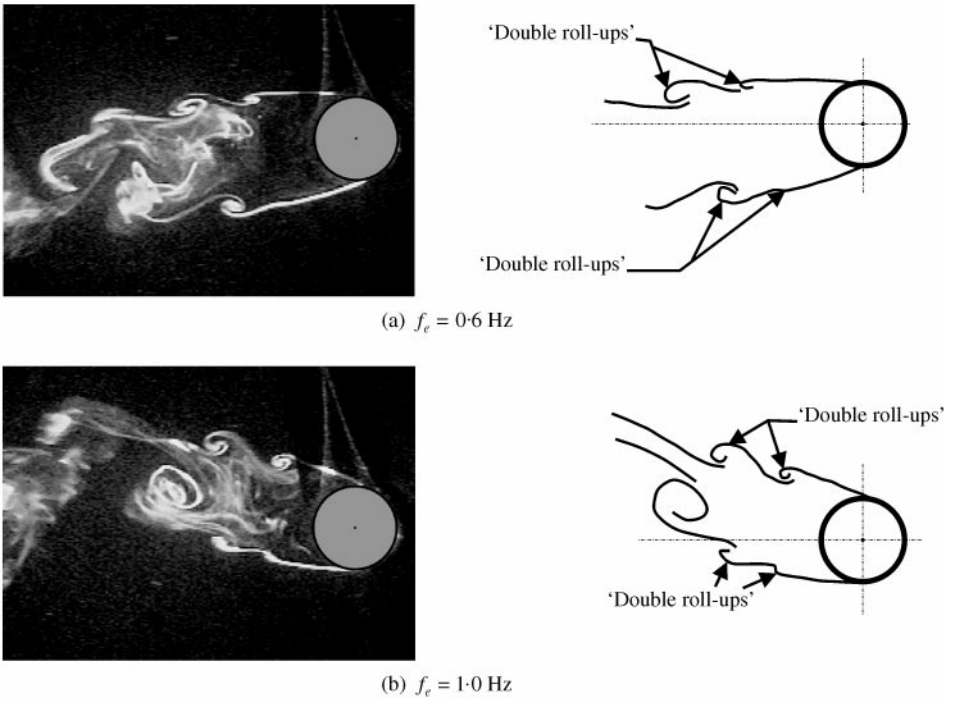

Figure 4. Visualized images (left) and tracings (right) illustrating the abrupt formation of *double roll-ups* in the shear layers, caused by acceleration of the oscillating cylinder: (a) $f_e = 0{\cdot}6$ Hz, (b) $f_e = 1{\cdot}0$ Hz.

Several vortex roll-ups occurred in the formation region in one oscillation cycle when the cylinder was forced to oscillate, primarily due to the influence of cylinder acceleration. The vortices from the two shear layers interacted in the near-wake through processes such as pairing and coalescence, both before and after they were shed. While the vortices were formed in a laminar fashion from the shear layers (at least at the lower excitation frequencies below the lock-in range), interaction between the vortices just before they were shed quickly destroyed their laminar nature, and the dye was dispersed rapidly. Therefore, visualization of vortices shed from the oscillating cylinder was not as good as that of the stationary cylinder. Furthermore, small-scale Kelvin–Helmholtz vortices which were absent

for the stationary cylinder, were sometimes observed on the shear layers when the cylinder was forced to oscillate. These small-scale vortices did not affect the process of vortex shedding significantly.

Synchronization of vortex shedding with cylinder motion is seen to occur in the visualizations when the vortex shedding process from the shear layers repeats itself every cycle (or its multiple, for 3-superharmonic excitation) of cylinder oscillation. Vortex formation from the shear layers is modified by cylinder acceleration when the cylinder is forced to oscillate (compare Figures 3 and 4), as evidenced by the formation of double roll-ups on the shear layers every half-cycle. This modification process caused by cylinder acceleration is synchronized with the vortex shedding process when lock-in occurs. In the current experiments, synchronization of vortex shedding with cylinder motion in the formation region was observed for the following cases: (a) $\frac{1}{3}$-subharmonic synchronization at $f_e = 0{\cdot}4$ Hz ($f_eD/U = 0{\cdot}067$); (b) $\frac{1}{2}$-subharmonic synchronization at $f_e = 0{\cdot}6$ Hz ($f_eD/U = 0{\cdot}10$); (c) fundamental lock-in (synchronization) at $f_e = 0{\cdot}9$, $1{\cdot}0$, $1{\cdot}1$, $1{\cdot}2$ and $1{\cdot}3$ Hz, spanning a reduced frequency range of $0{\cdot}15 \leq f_eD/U \leq 0{\cdot}22$; and (d) 3-superharmonic synchronization at $f_e = 2{\cdot}8$ Hz ($f_eD/U = 0{\cdot}47$) and $f_e = 3{\cdot}0$ Hz ($f_eD/U = 0{\cdot}50$). Results for synchronization in the formation region are discussed individually later in this section, in terms of periodic repetition of the dye structure in the formation region.

Synchronization of vortex shedding with cylinder motion (in the formation region) does not necessarily result in a 'synchronized wake pattern'. Williamson & Roshko (1988) discuss synchronization in their experiments in terms of wake patterns, which evolve in a manner that is periodic and synchronized with cylinder motion. In order to assess synchronized vortex shedding in terms of wake vortex patterns, experiments were conducted with a larger field of view, revealing the vortex street behind the cylinder. When synchronized wake patterns occurred in the current experiments, the dye was not dispersed from the vortex cores as easily as it would otherwise, since synchronization caused the vortices to be coherent during every cycle of cylinder oscillation. During excitation within synchronized regimes, the topology of the wake pattern was consistently preserved over a long duration of time. Vortices were shed into the evolving wake pattern in a manner that was synchronized with cylinder motion. For cylinder excitation at an amplitude ratio of $A/D = 0{\cdot}22$, Williamson & Roshko (1988) observed synchronized wake patterns for the following cases: (i) 2P + 2S-type wake pattern for the case of $\frac{1}{3}$-subharmonic excitation ($f_e/f_{0s} \approx 1/3$); (ii) 2P-type wake pattern for $0{\cdot}16 \leq f_eD/U \leq 0{\cdot}18$ and 2S-type wake pattern for $0{\cdot}18 \leq f_eD/U \leq 0{\cdot}23$, both occurring within the fundamental lock-in regime; (iii) C(2S)-type wake pattern, which is formed when coalescence of vortices in the near wake subsequently gives rise to a 2S vortex street, for $f_eD/U > 0{\cdot}23$.

To facilitate discussion of the visualization results, the oscillation frequency range $0.4 \text{ Hz} \leq f_e \leq 3{\cdot}0$ Hz is broken up into (i) 'fundamental lock-in regime' ($0{\cdot}9$ Hz $\leq f_e \leq 1{\cdot}3$ Hz); (ii) '$\frac{1}{3}$-subharmonic excitation' ($f_e = 0{\cdot}4$ Hz); (iii) '$\frac{1}{2}$-subharmonic excitation' ($f_e = 0{\cdot}6$ Hz); (iv) 'intermediate excitation frequencies' covering transition to the fundamental lock-in regime ($f_e = 0{\cdot}7$, $0{\cdot}8$ and $1{\cdot}4$ Hz); (v) 'higher excitation frequencies' beyond the lock-in regime ($f_e \geq 1{\cdot}5$ Hz).

4.1. Fundamental Lock-in Regime

Based on observations from the recorded video of the formation region, it was determined that fundamental lock-in occurred in the experimental runs with $f_e = 0{\cdot}9$, $1{\cdot}0$, $1{\cdot}1$, $1{\cdot}2$ and $1{\cdot}3$ Hz, spanning a reduced frequency range of $0{\cdot}15 \leq f_eD/U \leq 0{\cdot}22$. For cylinder excitation at these frequencies, vortex shedding from the shear layers was synchronized with cylinder motion during every cycle of cylinder oscillation. Furthermore, the experimental runs at

$f_e = 0{\cdot}9$ and $1{\cdot}0$ Hz, spanning a reduced frequency range of $0{\cdot}15 \leq f_e D/U \leq 0{\cdot}17$, belong to the 2P wake pattern regime, while those at $f_e = 1{\cdot}1$, $1{\cdot}2$ and $1{\cdot}3$ Hz, spanning a reduced frequency range of $0{\cdot}18 \leq f_e D/U \leq 0{\cdot}22$, belong to the 2S wake pattern regime.

A larger region of the wake was visualized in this range of reduced frequency in order to assess the wake vortex patterns. Figures 5–7 show both flow visualization images and tracings of the wake vortex patterns at reduced frequencies $f_e D/U$ of 0, $0{\cdot}16$ and $0{\cdot}2$, corresponding to a stationary cylinder, excitation in the 2P regime and excitation in the 2S regime, respectively. The wake pattern is clearly seen to be of 2P-type in Figure 6. Two vortex pairs are shed per cycle of cylinder oscillation, and the vortex pairs rapidly diverge away from the wake axis. The 2P wake pattern at $t^* = 1$ is seen as a replica of the wake pattern at $t^* = 0$, indicating synchronization with respect to cylinder motion. The 2S-type wake pattern shown in Figure 7, where two vortices are shed from the cylinder per cycle of cylinder oscillation, is markedly different from the 2P wake pattern shown in Figure 6. Instead, the 2S-type pattern is similar to the classical wake pattern behind the stationary

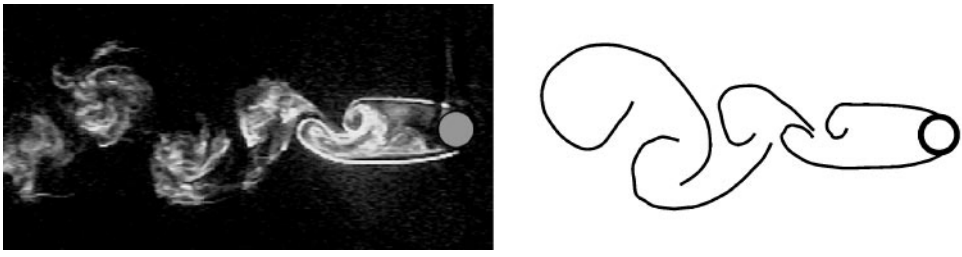

Figure 5. Visualized image (left) and tracing (right) of the wake vortex pattern behind the stationary cylinder.

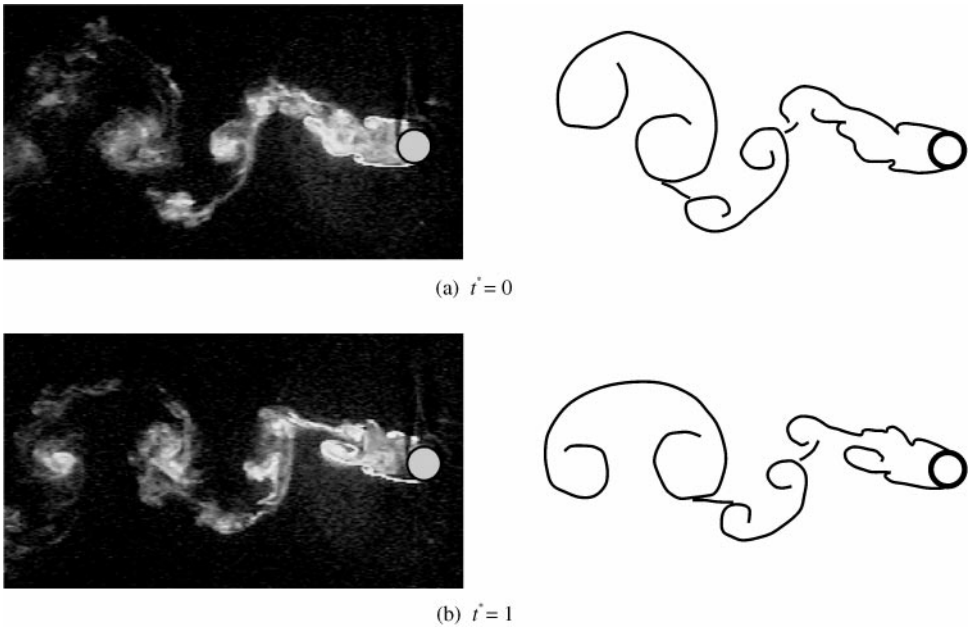

Figure 6. Visualized images (left) and tracings (right) of the wake vortex pattern behind the oscillating cylinder showing a 2P-type synchronized wake pattern at $f_e D/U = 0{\cdot}16$. Dimensionless time is $t^* = t/T_e$.

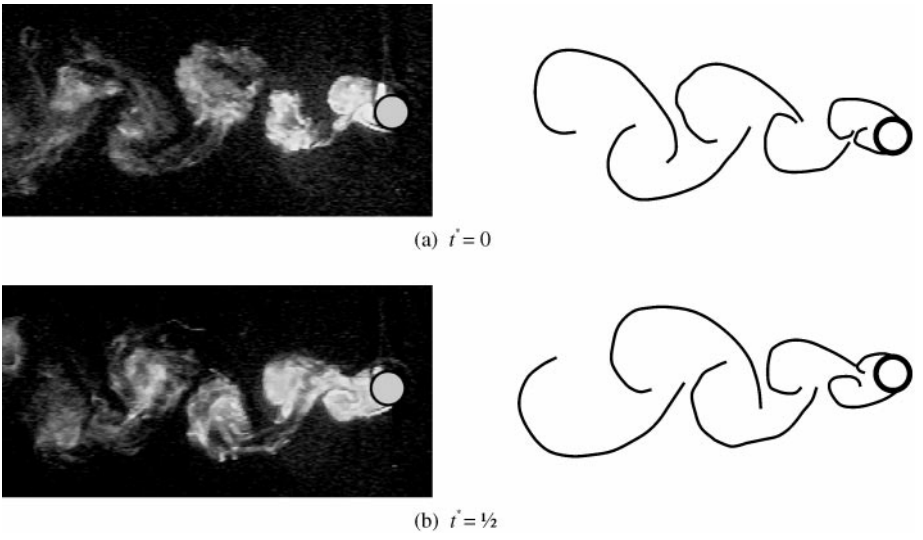

Figure 7. Visualized images (left) and tracings (right) of the wake vortex pattern behind the oscillating cylinder showing a 2S-type synchronized wake pattern at $f_eD/U = 0{\cdot}20$. Dimensionless time $t^* = t/T_e$.

cylinder shown in Figure 5, and the vortices remain close to the wake axis as they propagate downstream. The wake pattern at $t^* = 1/2$ is seen as a mirror image of the wake pattern at $t^* = 0$ in Figure 7, indicating synchronization with respect to cylinder motion. The coherent synchronized wake vortex patterns, which were observed for excitation frequencies within the fundamental lock-in regime (composed of the 2P and 2S regimes), could not be seen at frequencies either lower or higher than the bounds of the fundamental lock-in regime. For these cases of excitation just outside the lock-in range, the evolution of the vortex patterns was neither synchronized with cylinder motion nor preserved over several oscillation cycles.

Flow visualization results and corresponding tracings of the formation region, illustrating its evolution over one period of cylinder oscillation T_e, are given in Figures 8–11, corresponding to oscillation frequencies f_e of 1·0 Hz ($f_eD/U = 0{\cdot}17$), 1·1 Hz ($f_eD/U = 0{\cdot}18$), 1·2 Hz ($f_eD/U = 0{\cdot}20$) and 1·5 Hz ($f_eD/U = 0{\cdot}25$), respectively. In Figures 8–10, the cylinder is at bottom-dead-centre (bottom end of the stroke) at dimensionless time $t^* = 0$. In Figure 11, the cylinder position at $t^* = 0$ is arbitrary. Comparing the traces corresponding to $t^* = 0$ and $t^* = 1$ in each of these figures shows that vortex shedding is synchronized with cylinder motion in all the figures except Figure 11 ($f_e = 1{\cdot}5$ Hz), which is for a case when the frequency is just outside the lock-in regime.

For the excitation in the 2P regime illustrated in Figure 8, two like-signed vortices of counterclockwise sense are shed from the upper shear layer during the first half-cycle, as the cylinder proceeds from one position of zero-crossing ($t^* = \frac{1}{4}$ in Figure 8), via top-dead-centre, to the subsequent position of zero-crossing ($t^* = \frac{3}{4}$). Two like-signed vortices of clockwise sense are shed from the lower shear layer during the next half-cycle. The four vortices shed per cycle of cylinder oscillation propagate downstream as two vortex pairs that diverge away from the wake axis. Conversely, for excitation in the 2S regime illustrated in Figures 9 and 10, only two vortices are shed with every cycle of cylinder oscillation. The vortices are alternately shed from the two shear layers, immediately behind the cylinder.

Transition from the 2P-regime to the 2S-regime occurred between $f_e = 1{\cdot}0$ Hz and $f_e = 1{\cdot}1$ Hz, at a reduced frequency between 0·17 and 0·18. The critical frequency corresponding to transition from 2P- to 2S-type wake was seen in the current experiments to

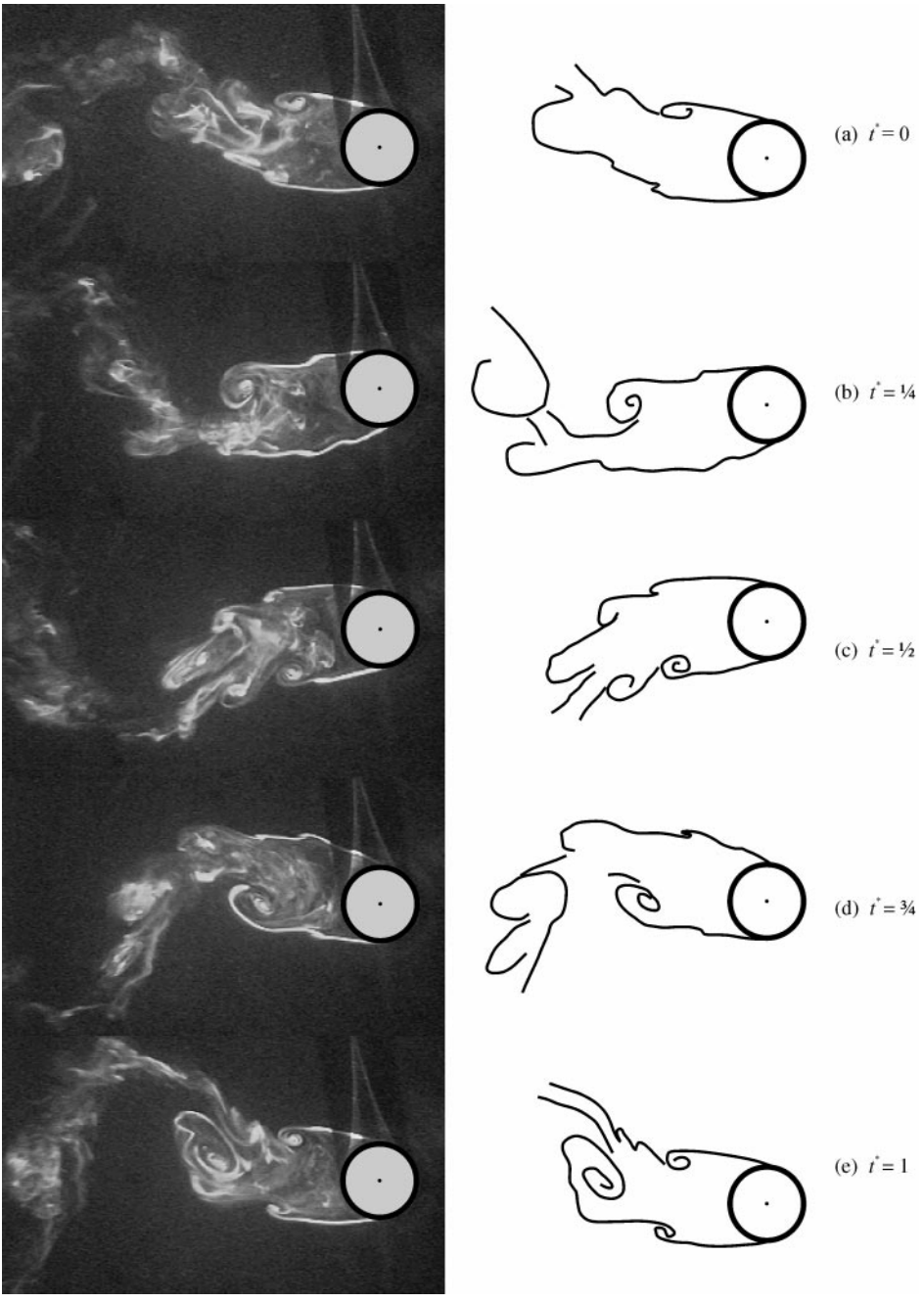

Figure 8. Visualized images (left) and tracings (right) showing the evolution of the vortex formation region behind the oscillating cylinder over one period of oscillation: $f_e = 1{\cdot}0$ Hz (fundamental lock-in/synchronization regime — 2P wake vortex pattern). Dimensionless time $t^* = t/T_e$. The cylinder is at bottom-dead-centre at time $t^* = 0$.

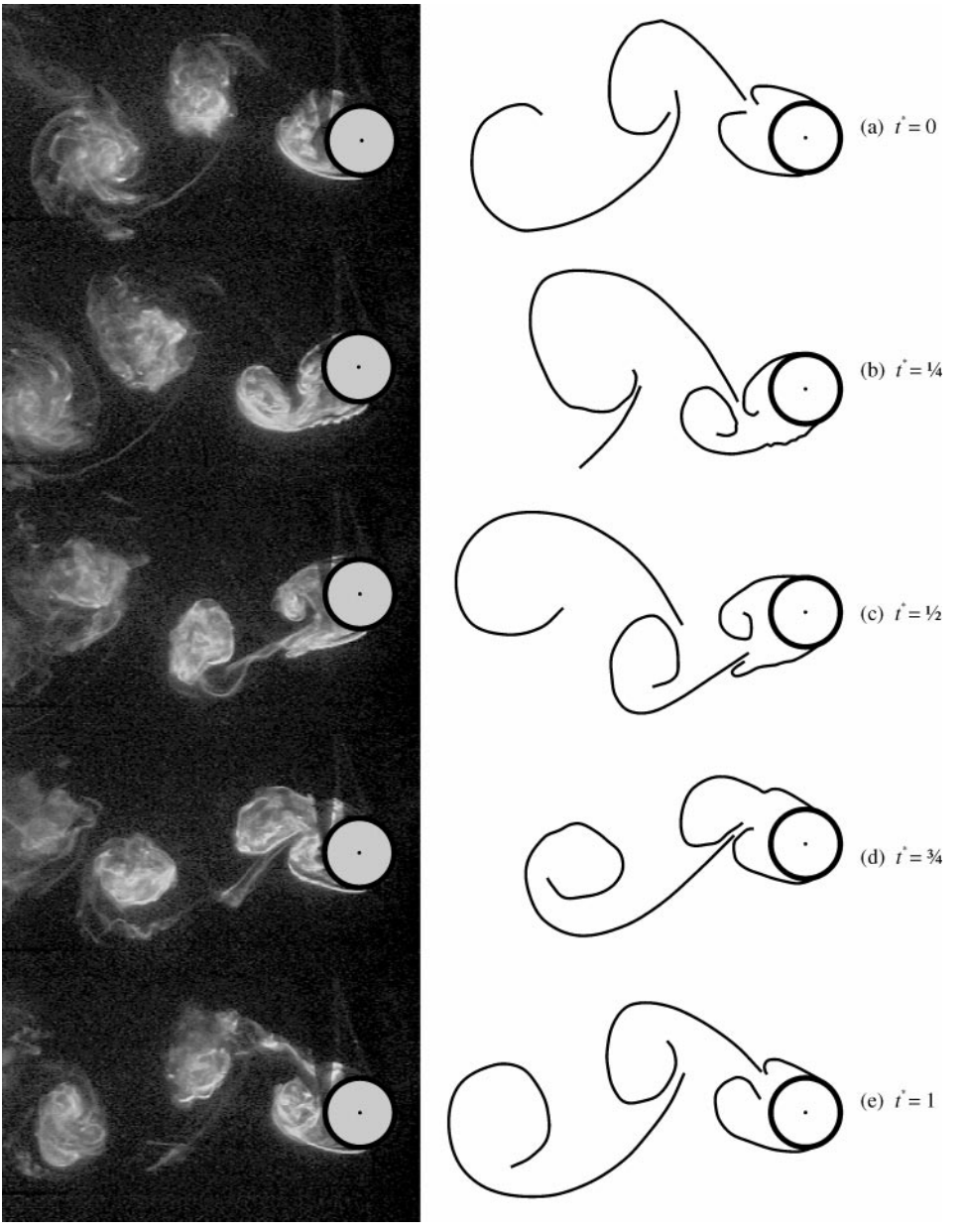

Figure 9. Visualized images (left) and tracings (right) showing the evolution of the vortex formation region behind the oscillating cylinder over one period of oscillation: $f_e = 1{\cdot}1$ Hz, corresponding to resonant synchronization (fundamental lock-in regime — 2S wake vortex pattern). Dimensionless time $t^* = t/T_e$. The cylinder is at bottom-dead-centre at time $t^* = 0$.

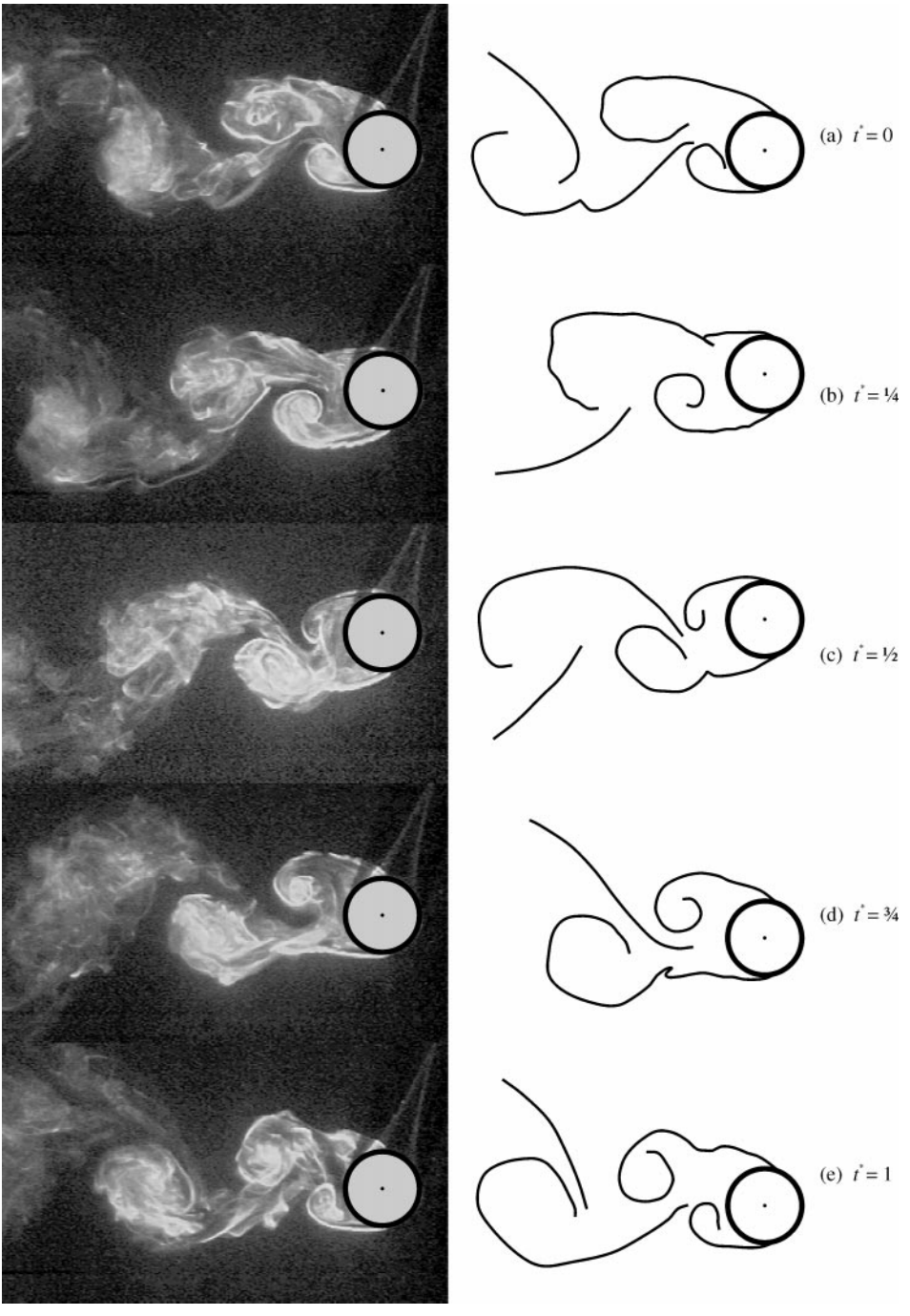

Figure 10. Visualized images (left) and tracings (right) showing the evolution of the vortex formation region behind the oscillating cylinder over one period of oscillation: $f_e = 1{\cdot}2$ Hz, showing a cycle of cylinder oscillation in which 'out-of-phase' vortex shedding occurs (fundamental lock-in regime — 2S wake vortex pattern). Dimensionless time $t^* = t/T_e$. The cylinder is at bottom-dead-centre at time $t^* = 0$.

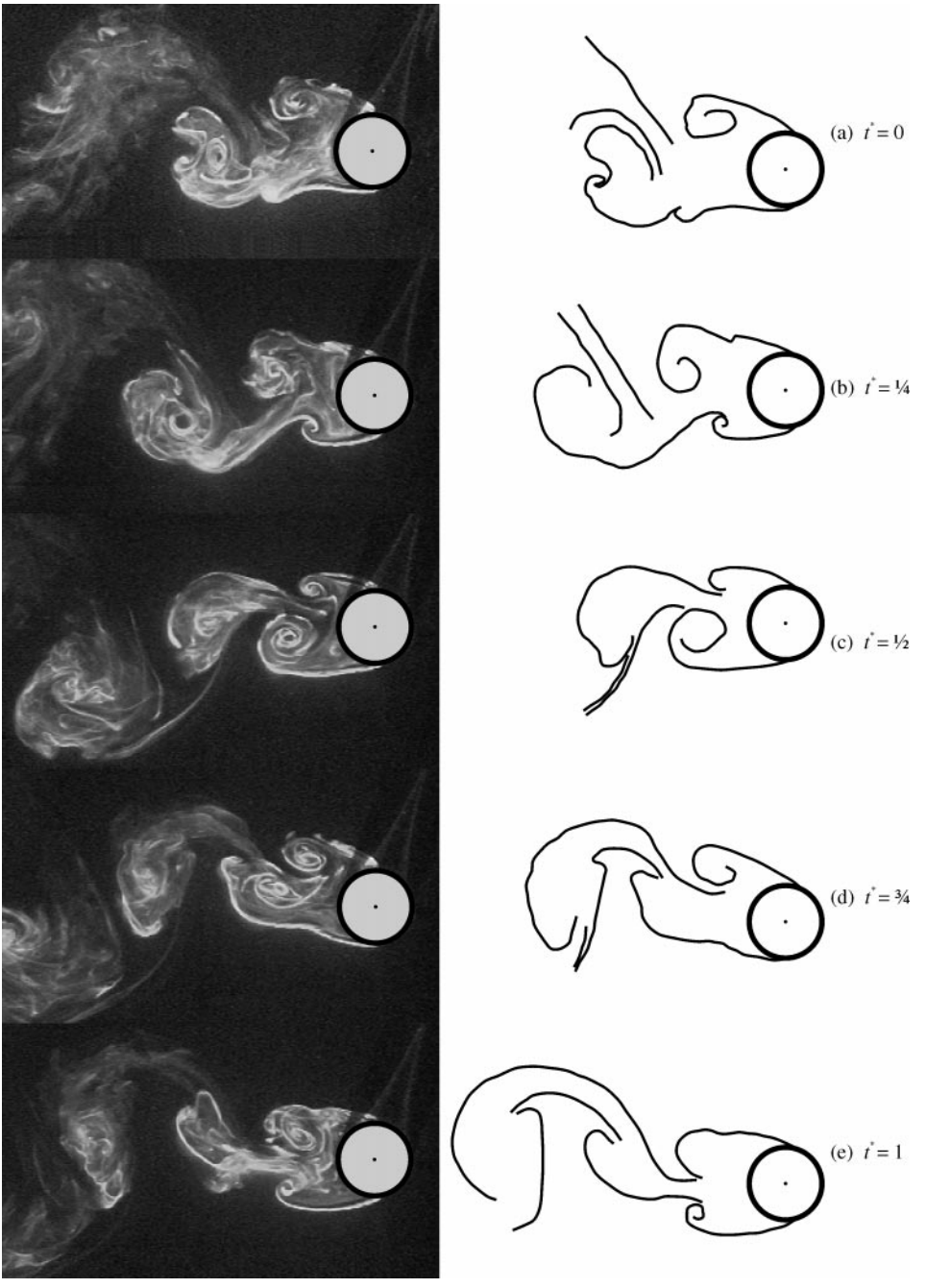

Figure 11. Visualized images (left) and tracings (right) showing the evolution of the vortex formation region behind the oscillating cylinder over one period of oscillation: $f_e = 1{\cdot}5$ Hz, vortex shedding is not synchronized with cylinder motion. Dimensionless time $t^* = t/T_e$. The cylinder is at some arbitrary position in its motion cycle at time $t^* = 0$.

induce dramatic reduction in vortex formation length, as can be seen by comparing Figures 8 and 9. The phase of vortex shedding relative to cylinder displacement, however, does not undergo a change during transition from the 2P-regime to the 2S-regime. This is evident by comparing Figures 8(a) and 9(a), when the cylinder is at bottom-dead-center or Figures 8(c) and 9(c), when the cylinder is at top-dead-center.

In the present experiments, the phase of vortex shedding relative to cylinder displacement switched by approximately π when f_e was increased past the resonant synchronization at 1·1 Hz. This phase switch phenomenon is illustrated in Figure 12, showing flow visualization images and tracings for $f_e = 1{\cdot}1$ and 1·2 Hz. Vortex shedding occurred 'in-phase' with cylinder motion at $f_e = 1{\cdot}1$ Hz as shown in Figure 12(a) ($f_eD/U = 0{\cdot}18$, $f_e/f_{0s} = 0{\cdot}87$), and 'out-of-phase' with cylinder motion at $f_e = 1{\cdot}3$ Hz ($f_eD/U = 0{\cdot}22$, $f_e/f_{0s} = 1{\cdot}02$). At $f_e = 1{\cdot}2$ Hz ($f_eD/U = 0{\cdot}20$, $f_e/f_{0s} = 0{\cdot}95$), vortex shedding was observed to be in-phase with cylinder motion [see Figure 12(c)] for some cycles of cylinder oscillation but out-of-phase [see Figure 12(b)] for other cycles. Over several cycles of cylinder oscillation, 'in-phase' and 'out-of-phase' vortex shedding occurred in a random manner. This 'bistable behaviour' at $f_e = 1{\cdot}2$ Hz may possibly be associated with the 'weakly chaotic relaxation oscillator regime' observed in the 2-D computations of Blackburn & Henderson (1999) for $0{\cdot}905 < f_e/f_{0s} < 0{\cdot}95$. Thus, Figure 12 illustrates not only the phase switch caused by increasing f_e from 1·1 to 1·2 Hz, but also the bistable behaviour of the vortex shedding process at $f_e = 1{\cdot}2$ Hz.

Incidentally, the flow visualization result for $f_e = 1{\cdot}2$ Hz shown in Figure 10 spans an oscillation *cycle* in which vortex shedding is *out-of-phase* with respect to the cylinder motion. One may compare Figures 9(a) and 10(a) where the cylinder is approximately at bottom-dead-centre, or Figures 9(c) and 10(c) where the cylinder is approximately at top-dead-centre, to see the phase switch as f_e is increased from 1·1 to 1·2 Hz. One must also note that for $f_e = 1{\cdot}2$ Hz, a flow visualization result similar to Figure 10, but showing in-phase shedding, can be obtained by appropriate choice of the oscillation cycle.

4.2. $\frac{1}{3}$-Subharmonic Excitation

The experimental run with $f_e = 0{\cdot}4$ Hz was close to the $\frac{1}{3}$-subharmonic excitation, for which $f_e = \frac{1}{3}f_{0s}$. Images showing the evolution of the vortex formation region over one period of oscillation of the cylinder are given in Figure 13. The cylinder is at bottom-dead-centre (bottom end of the stroke) at $t^* = 0$ and 1, and at top-dead-centre at $t^* = \frac{1}{2}$. The nominal structure of the formation region is repeated with every cycle of cylinder oscillation, the image corresponding to $t^* = 1$ is similar to that for $t^* = 0$. In order to generate the 2P + 2S wake vortex pattern of Williamson & Roshko, six vortices would have to be shed per cycle of cylinder oscillation. The acceleration of the cylinder each half-cycle gives rise to four vortices per cycle (the *double roll-ups* observed in the present experiments coalesce as they are shed). Two more vortices are generated from the shear layers by mechanisms pertaining to a stationary cylinder [as discussed in Gerrard (1966)] during the relatively long segments of the oscillation cycle when the cylinder has relatively little acceleration. Visualization was carried out with a larger field of view in order to observe the wake pattern, as described earlier for the fundamental lock-in regime. A coherent wake pattern synchronized with the cylinder motion was observed; i.e., the wake pattern at $t^* = 1$, 2, 3, etc. were replicas of the wake pattern at $t^* = 0$, as discussed before for the 2P-regime. However, since individual vortices could not be clearly seen, it was not possible to determine whether the wake pattern was of 2P + 2S-type.

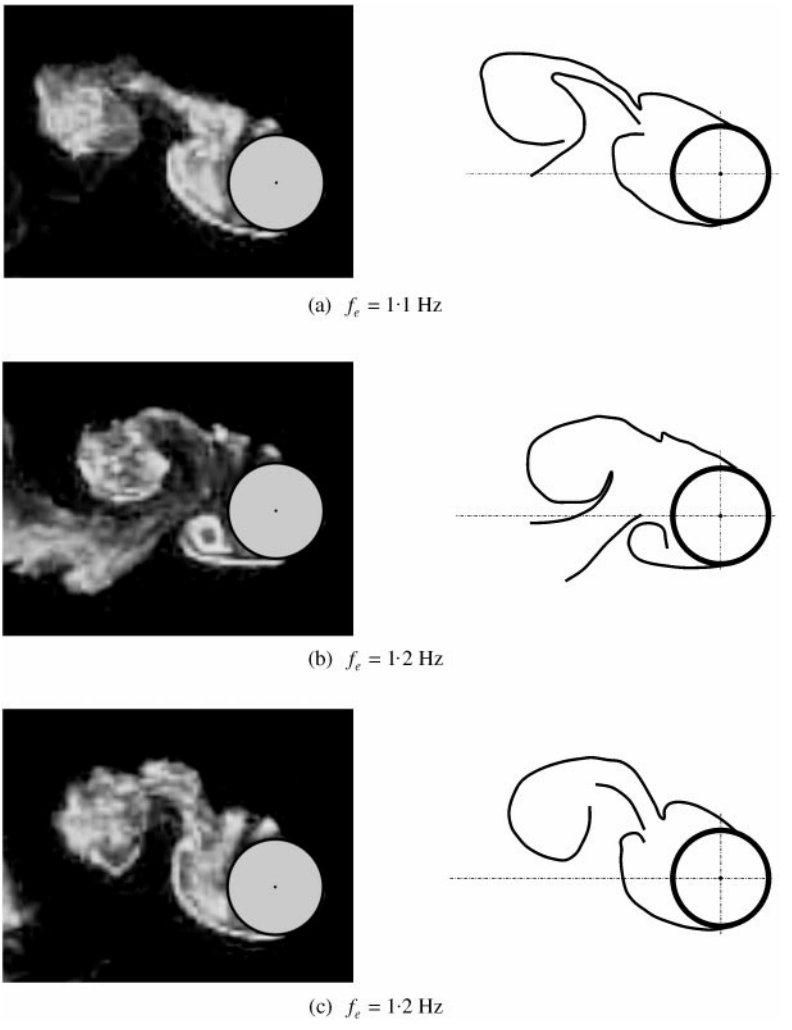

Figure 12. Visualized images (left) and tracings (right) illustrating the phenomenon in which the phase of vortex shedding relative to cylinder motion switches by approximately π within the fundamental lock-in regime. The cylinder is at bottom-dead-centre in all the images/tracings. (a) State of resonant synchronization, $f_e = 1{\cdot}1$ Hz, 'in-phase' shedding; (b) $f_e = 1{\cdot}2$ Hz, 'out-of-phase' shedding; (c) $f_e = 1{\cdot}2$ Hz, 'in-phase' shedding.

4.3. $\frac{1}{2}$-Subharmonic Excitation

The experimental run with $f_e = 0{\cdot}6$ Hz was close to the $\frac{1}{2}$-subharmonic excitation, for which $f_e = \frac{1}{2} f_{0s}$. Images showing the evolution of the vortex formation region over one period of oscillation of the cylinder are given in Figure 14. The cylinder is at bottom-dead-centre (bottom end of the stroke) at $t^* = 0$ and 1, and at top-dead-centre at $t^* = \frac{1}{2}$. Synchronization of vortex formation with cylinder motion is evident by comparing the image at $t^* = 1$ with the image at $t^* = 0$. The vortex from the top shear layer is fully formed when the cylinder is at bottom-dead centre (out-of-phase relationship) and subsequently when the cylinder is at top-dead-centre (in-phase relationship). This aspect of $\frac{1}{2}$-subharmonic excitation was discussed by Ongoren & Rockwell (1988). Upon visualizing a larger region of the

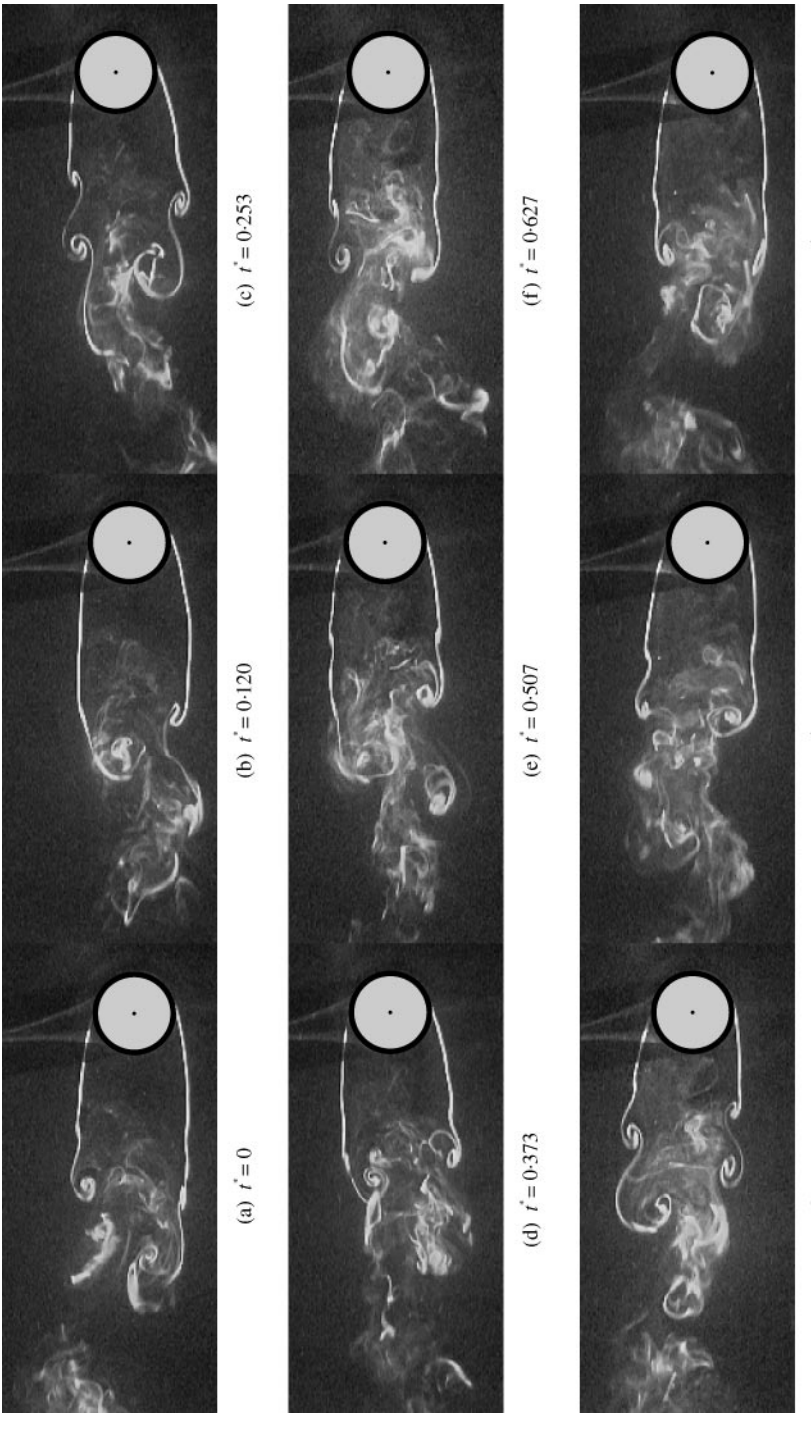

Figure 13. Images showing the evolution of the vortex formation region behind the oscillating cylinder over one period of oscillation: $f_e = 0{\cdot}4$ Hz corresponding to $\frac{1}{3}$-subharmonic synchronization. Dimensionless time $t^* = t/T_e$.

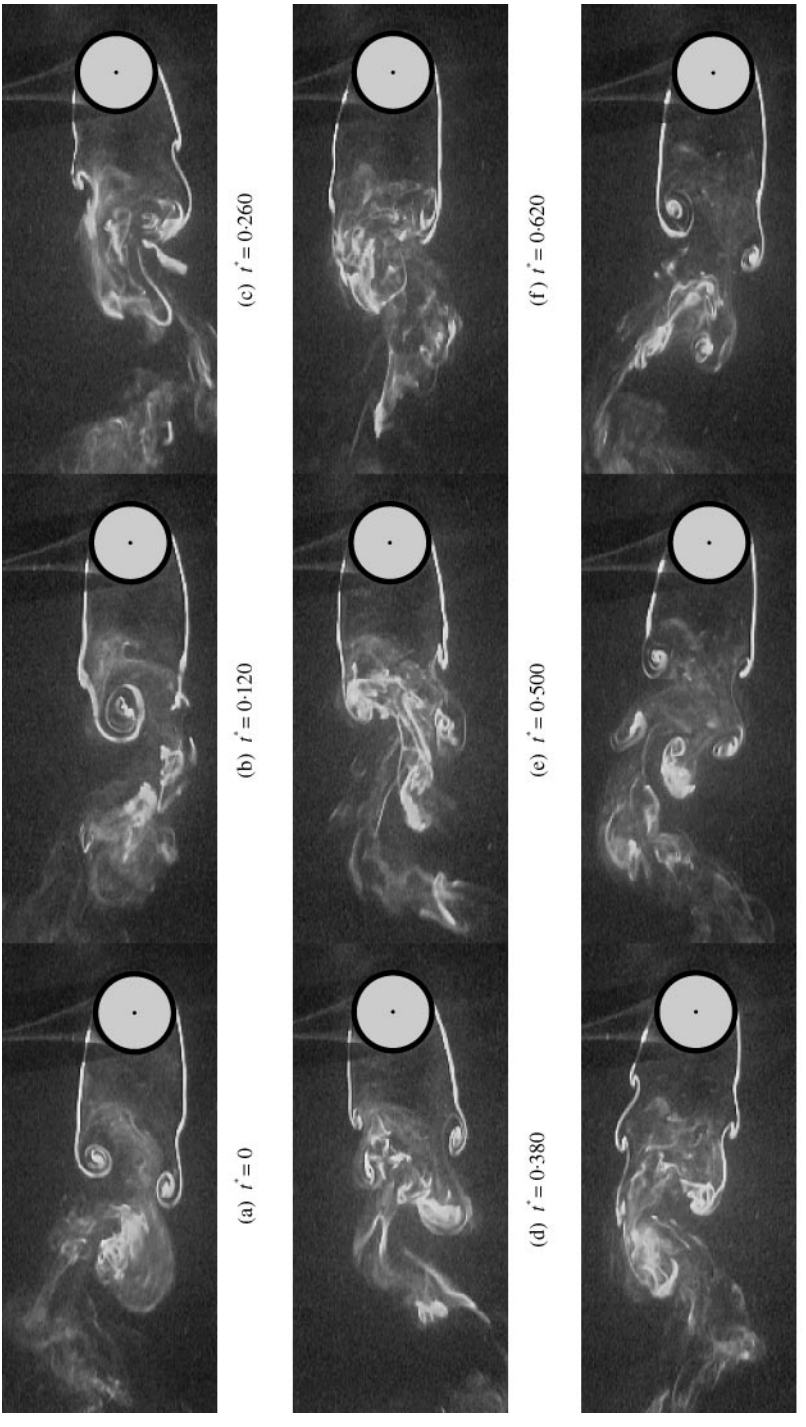

Figure 14. Images showing the evolution of the vortex formation region behind the oscillating cylinder over one period of oscillation: $f_e = 0{\cdot}6$ Hz corresponding to $\frac{1}{2}$-subharmonic synchronization in the formation region. Dimensionless time $t^* = t/T_e$.

wake, it was seen that a synchronized, coherent wake pattern was not formed. The wake vortices were observed to be coherent only during certain phases of the cylinder oscillation cycle.

4.4. Intermediate Excitation Frequencies

The results of the previous section suggest that for excitation in the range $0{\cdot}1 < f_e D/U < 0{\cdot}14$ and $0{\cdot}2 < f_e D/U < 0{\cdot}23$, the vortex shedding frequency switches between two (or more) values corresponding to locked-on and nonlocked-on states. At cylinder excitation frequencies of $f_e = 0{\cdot}7$ Hz ($f_e D/U = 0{\cdot}12$) and $f_e = 0{\cdot}8$ Hz ($f_e D/U = 0{\cdot}13$), representing the range between the $\frac{1}{2}$-subharmonic excitation and the onset of 2P regime, observation of the formation region indicated that vortex shedding was synchronized with cylinder motion for certain time spans (an order of magnitude longer than the period T_e), but that it occurred at a higher frequency at other times. The proportion of time for which the vortex shedding was synchronized with cylinder motion increased as the excitation frequency approached the locked-in range. Intermittent behaviour was also observed near the high frequency end of the fundamental lock-in regime, at $f_e = 1{\cdot}4$ Hz ($f_e D/U = 0{\cdot}23$).

For excitation at these intermediate frequencies, while the vortex shedding process was synchronized with cylinder motion for certain time spans, coherent wake patterns that were preserved over long time spans did not occur.

4.5. Higher Excitation Frequencies

For excitation frequencies higher than those corresponding to the fundamental lock-in regime ($1{\cdot}5$ Hz $\leq f_e \leq 3{\cdot}0$ Hz), the wake pattern quickly relaxed to the usual Karman mode (C(2S)-type of Williamson & Roshko). Dynamics of the formation region may or may not be synchronized with cylinder motion in this range of excitation frequencies.

For the 3-superharmonic synchronization, which occurred at $f_e = 2{\cdot}8$–$3{\cdot}0$ Hz, the dynamics of the formation region were periodic with every third cycle of cylinder, and one vortex shedding cycle (of frequency f_0) was spanned by three cycles of cylinder oscillation. The size of the formation region ('stagnant region' behind the cylinder) was substantially reduced at these excitation frequencies. This is evident from Figure 15 where images of the evolution of the vortex formation region over three periods of oscillation of the cylinder, illustrating 3-superharmonic synchronization at $f_e = 3{\cdot}0$ Hz are presented. The cylinder is at bottom-dead-centre (bottom end of the stroke) at time $t^* = 0$, 1, 2 and 3. The structure of the formation region at $t^* = 0$ is repeated only at $t^* = 3$.

A reduction in the size of the formation region did not occur at any of the other higher excitation frequencies considered. However, an interesting type of synchronization phenomenon was observed at $f_e = 1{\cdot}5$ Hz, corresponding to 1.5-nonharmonic synchronization. A coherent pair of vortices was observed at $t^* = 0$ just downstream of the formation region. Subsequent coherent vortex pairs occurred only at $t^* = 3$, 6, 9 etc. The current visualizations did not display 2-superharmonic synchronization.

4.6. Vortex Formation Length

An attempt to quantify vortex formation lengths for cylinder oscillation frequencies in the range $0{\cdot}4$ Hz $\leq f_e \leq 1{\cdot}5$ Hz is now discussed. While the vortex formation length is well defined for flow past a stationary cylinder, complications arise when the cylinder is forced to oscillate (at sufficiently large amplitude), for the following reasons.

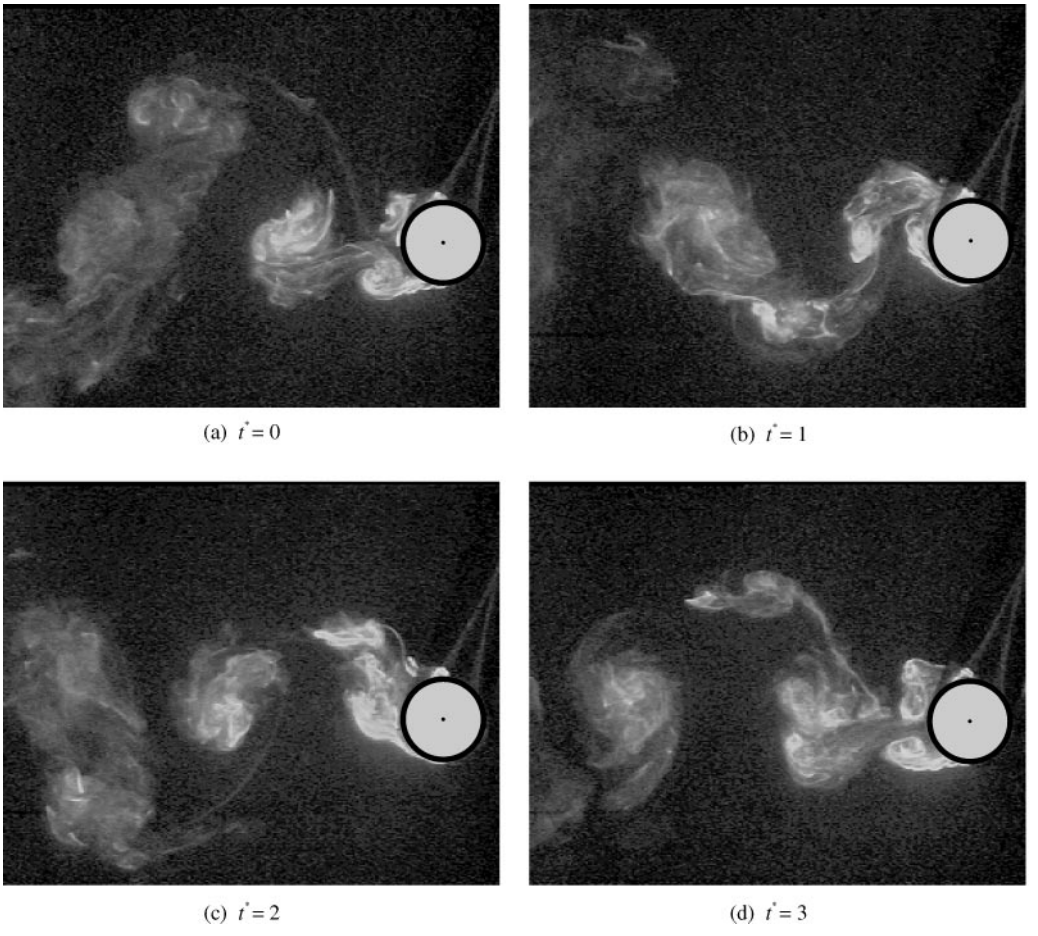

Figure 15. Images showing the evolution of the vortex formation region behind the oscillating cylinder over three periods of oscillation: $f_e = 3{\cdot}0$ Hz corresponding to 3-superharmonic synchronization in the formation region. Dimensionless time $t^* = t/T_e$.

(i) The shear layers shed from the cylinder *swing* up and down as the cylinder oscillates.

(ii) There are two distinct processes contributing to vortex formation: (a) those applicable to vortex formation from a stationary cylinder (Gerrard 1966), and (b) vortex roll-ups in the shear layers (in the form of *double roll-ups*) induced by acceleration of oscillating cylinder. Hence, the vortex formation length depends on the process which gives rise to the vortex, and vortices are not necessarily shed at the same streamwise location behind the cylinder.

(iii) More than two vortices are shed per cycle of cylinder oscillation for frequencies less than that of resonant synchronization. The manner in which the vortices formed from the shear layers interact (both before and after they are shed) is quite complex.

Representative vortex formation lengths L_f (where L_f is the streamwise distance from the axis of the cylinder to the core of a fully formed vortex) at various oscillation frequencies were determined from images of the formation region in which a fully formed vortex was clearly seen while the shear layers were approximately *horizontal*; for instance, see Figures 10(b), 13(b) and 14(a). The results are plotted in Figure 16. The vortex formation length for the $\frac{1}{3}$-subharmonic excitation (0·4 Hz) is roughly the same as that for a stationary cylinder ($L_f/D = 2{\cdot}6$). As the forcing frequency is increased the formation length becomes

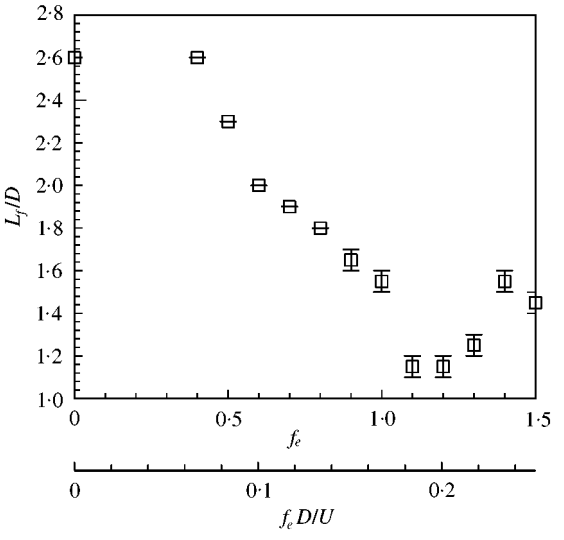

Figure 16. Representative dimensionless vortex formation lengths (square symbols, with error bars). The vortex formation length L_f is measured relative to the cylinder axis in the streamwise direction.

progressively smaller, until it reaches a minimum of $L_f/D = 1{\cdot}1$–$1{\cdot}2$ at $f_e = 1{\cdot}1$–$1{\cdot}2$ Hz, during resonant synchronization. The formation length decreases sharply as forcing frequency is increased from 1·0 Hz (2P-type wake) to 1·1 Hz (2S-type wake), at which point vortex formation occurs immediately behind the cylinder. As the frequency is increased above 1·2 Hz, the formation length starts increasing again.

5. DISCUSSION AND CONCLUSIONS

The main conclusions obtained from this work are outlined in the following.

1. Synchronized *wake patterns* which are repeated for every cycle of cylinder oscillation are observed for $\frac{1}{3}$-subharmonic excitation ($f_e = \frac{1}{3} f_{0s}$), and within the fundamental lock-in regime. Within the fundamental lock-in regime, at lower excitation frequencies, the 2P wake pattern results. Vortices shed from the cylinder quickly organize themselves and pair-up to give rise to a vortex street. The vortex pairs rapidly convect away from the wake centreline as they proceed downstream. When a critical excitation frequency is crossed within the fundamental locked-in regime, the 2S wake pattern results. Upon just crossing the critical frequency from the 2P to the 2S regime, the wake is said to be in a state of resonant synchronization in which exactly two vortices are shed from the cylinder each cycle; the vortex formation length correspondingly decreases sharply.

As the excitation frequency is further increased (within the 2S regime), another 'upper' critical frequency (of around 1·2 Hz, corresponding to $f_e D/U = 0{\cdot}20$) is crossed, and the phase of vortex shedding with respect to cylinder motion switches by approximately π. Near the upper critical frequency, the phase switching phenomenon is *bistable*. (Such a claim has not been made in earlier experimental studies and the phase switching phenomenon is described as abrupt.) On further increase of the oscillation frequency within the 2S regime, the phase of vortex shedding with respect to cylinder motion remains at approximately π.

Synchronized vortex shedding is no longer observed when the oscillation frequency is increased beyond that corresponding to the 2S regime. However, the wake quickly relaxes into the usual antisymmetric Karman mode. The evolution of the wake is not 'strongly' synchronized anymore with cylinder motion (until the 3-superharmonic synchronization

regime is encountered). Also, in these unsynchronized regimes, depending on their phase, some of the vortices in the vortex-street are more coherent than others.

In our visualization experiments, the excitation frequency range corresponding to the 2P wake pattern was $0{\cdot}15 \leq f_e D/U \leq 0{\cdot}17$, and the frequency range corresponding to the 2S wake pattern was $0{\cdot}18 \leq f_e D/U \leq 0{\cdot}22$. The critical reduced frequency separating the two wake patterns is between 0·17 and 0·18. At an amplitude ratio of 0·22, Williamson & Roshko (1988) obtained the 2P-type wake pattern for $0{\cdot}16 \leq f_e D/U \leq 0{\cdot}18$, and the 2S-type wake pattern for $0{\cdot}18 \leq f_e D/U \leq 0{\cdot}23$. Blackburn & Henderson (1999) obtained the fundamental lock-in range as $0{\cdot}77 < f_e/f_{0s} < 1{\cdot}015$ from their 2-D computations at $\mathrm{Re} = 500$ and $A/D = 0{\cdot}25$. The experimental results of Stansby (1976) give $0{\cdot}67 < f_e/f_{0s} < 1{\cdot}4$, at $\mathrm{Re} = 3600$ and $A/D = 0{\cdot}22$. In the current experiments, we have $0{\cdot}71 < f_e/f_{0s} < 1{\cdot}02$ as the range for fundamental lock-in. The agreement between the various results is good. Stansby's larger range for lock-in may be due both to the larger Reynolds number in his experiments and to the fact that 'intermittent lock-in' is not easily evident at the high frequency end of the fundamental lock-in range.

2. A synchronized wake pattern is not observed for the $\frac{1}{2}$-subharmonic excitation. Williamson & Roshko (1988) use arguments regarding symmetry of the vortices in the vortex street to explain why a synchronized wake pattern is not possible for this case but is possible for the $\frac{1}{3}$-subharmonic excitation. Although a synchronized wake pattern is not observed, vortex formation from the shear layers is synchronized with cylinder motion for the $\frac{1}{2}$-subharmonic excitation, as discussed by Ongoren & Rockwell (1988). Thus, synchronization of the formation region and vortex shedding with cylinder oscillation does not imply the existence of corresponding synchronized, coherent wake pattern.

3. At intermediate frequencies between the fundamental locked-in regime and the $\frac{1}{2}$-subharmonic excitation, locked-in vortex shedding occurs intermittently with unsynchronized vortex shedding, as discussed previously by Stansby (1976). The duration for vortex shedding synchronized with cylinder motion increases as the fundamental lock-in regime is approached.

4. The acceleration phase of the cylinder (as it moves from the ends of the stroke towards its mean position) causes vortex roll-ups on the shear layers—a phenomenon that is especially evident for excitation frequencies less than that of resonant synchronization. In the current study, both shear layers develop abrupt *double roll-ups* as the cylinder accelerates from bottom-dead-centre to its mean position, and once again as the cylinder accelerates from top-dead-centre to its mean position. These roll-ups nominally interact in a manner similar to that of *single roll-ups* in the process of generating the vortex street.

5. For excitation frequencies higher than those corresponding to the fundamental locked-on regime, the wake pattern quickly relaxes to the usual Kármán mode. The dynamics in the formation region is not synchronized to cylinder motion except for the 3-superharmonic synchronization, when the near wake dynamics repeats itself every third cycle, and a coherent, synchronized wake pattern is formed. At higher excitation frequencies, the formation region shrinks to a minimum only during 3-superharmonic synchronization. Synchronization of the near wake for 2-superharmonic excitation is not evident in either the visualization or the hot film experiments.

6. Williamson & Roshko (1988) attribute the jump in the lift force magnitude and in the phase of the lift force within the fundamental locked-on regime to the sudden transition from 2P synchronization to 2S synchronization. Other studies, such as those of Stansby (1976), Zdravkovich (1982) and Ongoren & Rockwell (1988), indicate that the phase switching phenomenon (within the 2S synchronization regime) causes the jump in lift force magnitude and in the phase of the lift force relative to cylinder motion. Both the sudden transition from 2P to 2S synchronization and the phase switching phenomenon within the

2S regime are observed to occur in the present experiments. The critical frequency corresponding to the transition from the 2P–2S regimes is lower than the 'critical frequency' corresponding to the phase switching phenomenon. In the current experiments, the phase switch does not occur abruptly. Instead, over several cycles of cylinder oscillation, both 'in-phase' and 'out-of-phase' vortex shedding occur during the transition.

ACKNOWLEDGEMENTS

The authors gratefully acknowledge the support by the Natural Sciences and Engineering Research Council (NSERC) of Canada and Le Fonds FCAR of Québec.

REFERENCES

BEARMAN, P. W. 1984 Vortex shedding from oscillating bluff bodies. *Annual Review of Fluid Mechanics* **16,** 195–222.

BEARMAN, P. W. & CURRIE, I. G. 1979 Pressure-fluctuation measurements on an oscillating circular cylinder. *Journal of Fluid Mechanics* **91,** 661–677.

BLEVINS, R. D. 1977 *Flow-Induced Vibration.* Second edition, 1990. New York: Van Nostrand Reinhold.

BISHOP, R. E. D. & HASSAN, A. Y. 1964 The lift and drag forces on a circular cylinder oscillating in a flowing fluid. *Proceedings of the Royal Society* (*London*) Series A **277,** 51–75.

BLACKBURN, H. M. & HENDERSON, R. D. 1999 A study of two-dimensional flow past an oscillating cylinder. *Journal of Fluid Mechanics* **385,** 255–286.

BRIKA, D. & LANEVILLE, A. 1993 Vortex-induced vibrations of a long flexible cylinder. *Journal of Fluid Mechanics* **250,** 481–508.

CHEN, S. S. 1987a Flow-*Induced Vibration of Circular Cylindrical Structures.* Washington: Hemisphere Publishing.

CHEN, S. S. 1987b A general theory for dynamic instability of tube arrays in crossflow. *Journal of Fluids and Structures* **1,** 35–53.

DEN HARTOG, J. P. 1934 The vibration problem in engineering. In *Proceedings* 4*th International Congress of Theoretical and Applied Mechanics*, Cambridge, U.K., pp. 36–53.

FENG, C. C. 1968 The measurement of vortex-induced effects in flow past stationary and oscillating circular and D-section cylinders. Master's Thesis, University of British Columbia.

GERRARD, J. H. 1966 The mechanics of the formation region of vortices behind bluff bodies. *Journal of Fluid Mechanics* **25,** 401–413.

GRIFFIN, O. M. 1971 The unsteady wake of an oscillating cylinder at low Reynolds numbers. *Journal of Applied Mechanics* **38,** 729–738.

GRIFFIN, O. M. & RAMBERG, S. E. 1974 The vortex-street wakes of vibrating cylinders. *Journal of Fluid Mechanics* **66,** 533–576.

GRIFFIN, O. M. & VOTAW, C. W. 1972 The vortex street in the wake of a vibrating cylinder. *Journal of Fluid Mechanics* **51,** 31–48.

GU, W., CHYU, C. & ROCKWELL, D. 1994 Timing of vortex formation from an oscillating cylinder. *Physics of Fluids* **6,** 3677–3682.

KHALAK, A. & WILLIAMSON, C. H. K. 1996 Dynamics of a hydroelastic cylinder with very low mass and damping. *Journal of Fluids and Structures* **10,** 455–472.

KHALAK, A. & WILLIAMSON, C. H. K. 1997 Fluid forces and dynamics of a hydroelastic structure with very low mass and damping. *Journal of Fluids and Structures* **11,** 973–982.

KOOPMANN, G. H. 1967 The vortex wakes of vibrating cylinders at low Reynolds numbers. *Journal of Fluid Mechanics* **28,** 501–512.

LU, X.-Y. & DALTON, C. 1996 Calculation of the timing of vortex formation from an oscillating cylinder. *Journal of Fluids and Structures* **10,** 527–541

MAIR, W. A. & MAULL, D. J. 1971a Bluff bodies and vortex shedding—a report on Euromech 17. *Journal of Fluid Mechanics* **45,** 209–224.

MAIR, W. A. & MAULL, D. J. 1971b Aerodynamic behaviour of bodies in the wakes of other bodies. *Philosophical Transactions of the Royal Society* (*London*) A **269,** 425–437.

ONGOREN, A. & ROCKWELL, D. 1988 Flow structure from an oscillating cylinder. Part 1. Mechanisms of phase shift and recovery in the near wake. *Journal of Fluid Mechanics* **191,** 197–223.

PAÏDOUSSIS, M. P. 1980 Flow-induced vibrations in nuclear reactors and heat exchangers: practical experiences and state of knowledge. In *Practical Experiences with Flow Induced Vibrations* (eds E. NAUDASCHER & D. ROCKWELL), pp. 1–81. Berlin: Springer-Verlag.

PAÏDOUSSIS, M. P. 1981 Fluidelastic vibration of cylinder arrays in axial and cross-flow: state of the art. *Journal of Sound and Vibration* **76,** 329–360.

PAÏDOUSSIS, M. P. 1983 A review of the flow-induced vibrations in reactors and reactor components. *Nuclear Engineering and Design* **74,** 31–60.

PAÏDOUSSIS, M. P. 1993 Some curiosity-driven research in fluid-structure interactions and its current applications. Calvin Rice lecture. *ASME Journal of Pressure Vessel Technology* **115,** 2–14.

PARKINSON, G. V. 1989 Phenomena and modelling of flow-induced vibrations of bluff bodies. *Progress in Aerospace Science* **26,** 169–224.

PRICE, S. J. & SERDULA, C. 1995 Flow visualization of vortex shedding around multi-tube marine risers in a steady current. In *Flow Induced Vibration* (ed. P. W. BEARMAN), pp. 483–493. Amsterdam: A. A. Balkema.

SARPKAYA, T. 1979 Vortex-induced oscillations—a selective review. *Journal of Applied Mechanics* **46,** 241–258.

STANSBY, P. K. 1976 The locking-of vortex shedding due to the cross-stream vibration of circular cylinders in uniform and shear flows. *Journal of Fluid Mechanics* **74,** 641–655.

TOEBES, G. H. 1969 The unsteady flow and wake near an oscillating cylinder. *ASME Journal of Basic Engineering* **91,** 493–505.

WILLIAMSON, C. H. K. & ROSHKO, A. 1988 Vortex formation in the wake of an oscillating cylinder. *Journal of Fluids and Structures* **2,** 355–381.

ZDRAVKOVICH, M. M. 1982 Modification of vortex shedding in the synchronization range. *ASME Journal of Fluids Engineering* **104,** 513–517.